

PAPER • OPEN ACCESS

Colloidal rods in optical potential energy landscapes

To cite this article: Joshua L Abbott *et al* 2019 *J. Phys. D: Appl. Phys.* **52** 024002

View the [article online](#) for updates and enhancements.

Recent citations

- [Synthesis of Colloidal SU8 Polymer Rods Using Sonication](#)
Carla FernándezRico *et al*
- [Energy landscape of colloidal dumbbells in a periodic distribution of light](#)
E. Sarmiento-Gómez *et al*
- [Transport of a colloidal particle driven across a temporally oscillating optical potential energy landscape](#)
Joshua L Abbott *et al*



IOP | ebooks™

Bringing you innovative digital publishing with leading voices to create your essential collection of books in STEM research.

Start exploring the collection - download the first chapter of every title for free.

Colloidal rods in optical potential energy landscapes

Joshua L Abbott¹, James A Spiers¹, Yongxiang Gao^{1,2}, Dirk G A L Aarts¹
and Roel P A Dullens¹ 

¹ Department of Chemistry, Physical and Theoretical Chemistry Laboratory, University of Oxford, South Parks Road, Oxford, OX1 3QZ, United Kingdom

² Institute for Advanced Study, Shenzhen University, Nanhai Avenue 3688, Nanshan District, Shenzhen 518060, People's Republic of China

E-mail: roel.dullens@chem.ox.ac.uk

Received 24 May 2018, revised 24 September 2018

Accepted for publication 2 October 2018

Published 31 October 2018



Abstract

We study the static and dynamic behaviour of colloidal rods in an optical potential energy landscape. We explore the stable states of a colloidal rod in a single optical trap close to a flat wall. Here, two metastable states are observed, horizontal and vertical, both of which experience a parabolic potential energy landscape. Next we place a colloidal rod into a one-dimensional sinusoidal optical potential energy landscape and introduce a constant driving velocity. When driven below the critical velocity, the particle is confined to a single potential energy minimum of the optical landscape and the equilibrium position of a particle is investigated. The equilibrium position of a rod is found to vary substantially from that of a sphere, due to the drag coefficient of a rod being highly dependent on its proximity to an optical trap. The driving velocity is increased to enable the particle to traverse the periodic landscape and above the critical velocity, the average particle velocity increases as the square root of the driving velocity. When introducing oscillations to the driving velocity we observe dynamic mode locking and characterise the nature of synchronised motion of the rod-like particles.

Keywords: colloidal rods, dynamic mode locking, optical trapping, optical potential energy landscapes, nonlinear dynamics

(Some figures may appear in colour only in the online journal)

1. Introduction

Optical tweezers were first developed by Ashkin in the 1980s [1], after he initially observed the motion of microscopic particles when subject to a laser light source [2]. This has led to extensive research into the behaviour of a sphere in an optical trap [3–6]. Due to its isotropy, this is the most studied geometry which has resulted in applications in optical sorting [7–10], microrheology [11, 12], and protein folding [13]. Over the past 30 years, the field of optical trapping has hugely evolved [14–16] with the ability to impose angular momentum on particles with Laguerre–Gaussian modes [15, 17] and create Bessel beams which are ‘diffractionless’ [15]. It is also now possible to create a vast number of different shapes of micron sized particles that can be optically trapped [18, 19], yet many,

including intricate ‘colloidal molecules’, remain unexplored due to their complexity [20–23].

While anisotropic particles are more complex to study, their complexity leads to phenomena that are unseen for spheres. For example, the phase behaviour of rods differs from spheres and the bulk properties of spherocylinders and rods have been greatly explored both theoretically and experimentally [24–35]. For rods, the crystal and isotropic liquid phases are separated by a number of complex liquid crystal phases with varying degrees of translational and orientational order [25], which can have a complex interaction with light and cause birefringence [36].

Rods can also be manipulated using a variety of external fields [33, 37–39] giving rise to further complex phase behaviour such as string formation [33]. In general, however,



external fields such as gravitational fields [27], electric fields [40] or confinement [34, 41] affect the entire sample and do not have the same single particle resolution that can be achieved with an optical trap. Gaining a deeper understanding of the behaviour of rods is particularly relevant due to the ubiquity of microscopic rod-like objects, from the liquid crystal make up of electronic displays [42] to bacteria and virus filaments [43].

Previous works have investigated the behaviour of rod-shaped objects in single [44–47] and multiple optical traps [48], including nano-rods and nano-wires in optical fields [49, 50], where the anisotropy is shown to influence the trapping stability. Studies of colloidal spheres driven through an optical potential energy landscape [51] have shed light on a wide range of phenomena including kinetically locked-in transport [52], particle sorting [7–10], friction [53–55] and dynamic mode locking whereby particle motion synchronises with an external frequency [56–58]. However, for a rod driven through an optical potential energy landscape, synchronisation may be far more complex as the inherent anisotropy of a rod may lead to the potential for different modes of synchronisation.

Here we study the behaviour of a colloidal rod when confined in a single optical trap close to a flat wall. The arising metastable states are characterised, which correspond to a horizontal or vertical rod. We then introduce a colloidal rod to a periodic optical landscape formed of many optical traps and explore the motion in the case of a constant driving force. Here the effective drag of a rod and sphere greatly differ, which can be indirectly observed. Subsequently, a modulation to the driving force is introduced, leading to synchronisation. Particle motion is characterised for a dynamically mode locked particle and there is a clear similarity between rods and spheres in optical landscapes when driven above the critical velocity.

This paper is organised as follows: section 2 lays out the theoretical framework with a description of a colloidal particle driven through an optical landscape. The experimental system is described in section 3 with details of the particles and the optical landscapes that are used. Experimental results are discussed in section 4, initially for a static rod, and then for a rod driven through an optical landscape with both a constant and a modulated driving force.

2. Theoretical background

2.1. Optical trapping of colloidal rods

Here we consider a rod in an optical trap, which can behave differently to a sphere due to its inherent shape anisotropy. It is expected that the centre of the rod will be attracted to the point of highest laser intensity, which is the focus of the beam [1]. However, this does not define the orientation of a rod. In this respect it is important to note that in three-dimensional (3D) space, an optical trap is not fully symmetric, though it is in the two-dimensional (2D) cross-section perpendicular to the optical axis. Instead, a trap in 3D is elongated in the direction of the laser beam [6, 17] due to inherent optical effects and optical aberrations. A rod maximises its overlap with the

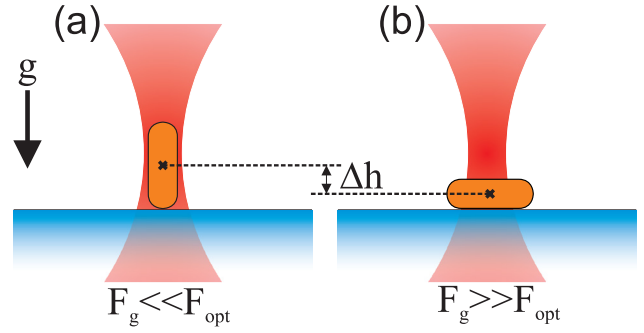


Figure 1. Schematic of a rod in an optical trap. (a) A rod is trapped vertically in the case where the optical forces dominate. (b) When gravity is the dominant force, a rod is trapped horizontally, where it minimises its gravitational potential energy. Δh shows the difference in height for the centre of mass of the rod.

region of highest intensity by aligning its major axis parallel to the optical axis (see figure 1(a)).

2.1.1. Gravitational effects. In our experimental system the rods have a much higher mass density than the solvent, meaning they are subject to a downward acting gravitational force that, for a perfect spherocylinder of length L and width W , is given by [59]

$$F_g = mg = \frac{\Delta\rho\pi g W^2}{4} \left(L + \frac{2}{3}W \right). \quad (1)$$

Here, $\Delta\rho$ is the mass density difference between the particle and the solvent. If we consider the position of a rod under gravity within an optical trap close to a wall, we can identify two limiting cases, corresponding to either the optical forces or gravity dominating. When the optical forces dominate, a rod will maximise its overlap with the laser beam by aligning with the optical axis in a vertical configuration as shown in figure 1(a). However, when gravity dominates, a particle will be confined to the plane next to the glass surface and be forced into a horizontal configuration as shown in figure 1(b). Note that the rod is still drawn into the centre of the optical trap in the xy -plane but is unable to lie in the centre of the trap in the z direction. The gravitational potential energy difference between these states is $F_g\Delta h = F_g L/2$, and is therefore dependent on the particle size.

2.2. Viscous drag on a rod

In a viscous fluid the motion of a rod is far more complex than that of a sphere due to its shape anisotropy. This anisotropy results in two possible modes of motion corresponding to parallel or perpendicular motion with respect to the long axis of the rod. The drag coefficient perpendicular to the rod's major axis is [60]

$$\zeta_{\perp} = \frac{4\pi\eta L}{(\sigma + \gamma_{\perp})}, \quad (2)$$

where η is the viscosity of the solvent and $\sigma = \ln(L/W)$. The value of the coefficient $\gamma_{\perp} \approx 1$ is found to vary slightly

amongst different theories. The drag coefficient for a rod moving collinear with the major axis is [60]

$$\zeta_{\parallel} = \frac{2\pi\eta L}{(\sigma + \gamma_{\parallel})}, \quad (3)$$

where the coefficient $\gamma_{\parallel} \approx -0.1$. It is worth noting from (2) and (3), that $\zeta_{\perp} > \zeta_{\parallel}$.

When a rod is brought close to a wall these expressions are no longer strictly valid as a wall restricts rod rotation and translation. Simulations have been carried out to study the behaviour of a rod in close proximity to a wall for an aspect ratio (L/W) of 10 [61]. The extent to which a wall affects rod motion is dependent on the relative angle of a rod, however, by assuming that the normal vector of the wall is perpendicular to the long axis of the rod, as shown in figure 1(b), the parallel drag coefficient ζ_{\parallel} can be approximated by [61]

$$\zeta_{\parallel}(z) \approx \zeta_{\parallel}^B \left[1 + 0.1015 \frac{W}{z} \right], \quad (4)$$

where $\zeta_{\parallel}(z)$ is now dependent on z , the distance between the rod and the wall. ζ_{\parallel}^B is the bulk parallel drag coefficient. When a rod is driven through an optical landscape it remains horizontal throughout experiments and motion is in the direction of the long axis so this is the only contribution that needs to be considered.

2.3. Motion of a colloidal rod in an optical potential energy landscape

A Langevin equation can be used to describe the motion of a Brownian particle driven through an optical potential energy landscape. In one dimension it can be expressed as

$$\zeta \frac{dx}{dt} = F_{DC} + F_{AC} \sin(2\pi\nu t) + F_{opt}(x) + \xi(t), \quad (5)$$

where ζ is the drag coefficient which is assumed to be constant and dx/dt is the particle velocity. The driving force consists of a constant term, F_{DC} , and a time-dependent term with an amplitude, F_{AC} . The Brownian noise is expressed as $\xi(t)$ and F_{opt} is the force due to the optical landscape which can be written more comprehensively for a line of optical traps with a small spacing, λ , as [57, 62]

$$F_{opt}(x) = -F_C \sin\left(\frac{2\pi x}{\lambda}\right). \quad (6)$$

The trap spacing, λ , corresponds to the wavelength of the optical landscape and F_C is the critical force which can be expressed as [62]

$$F_C = \frac{2(2\pi V_0)^{3/2}}{\lambda^2 k^{1/2}} \exp\left(-\frac{2\pi^2 V_0}{\lambda^2 k}\right), \quad (7)$$

where V_0 denotes the trap depth of each contributing optical trap, k is the associated trap stiffness. Equation (6) is true for a sphere, however, in one dimension the only distinction between a sphere and a rod is the particle length scale. This length scale is simply the radius for a sphere, and for a rod the

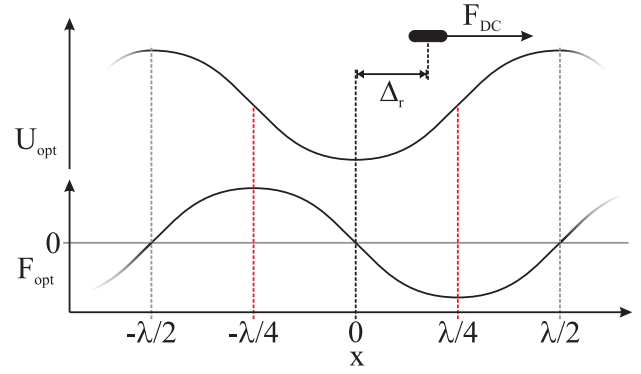


Figure 2. A schematic showing the optical potential energy landscape and the optical force landscape experienced by a rod or sphere. If F_{DC} is below the critical force then the particle is confined to a single minimum ($x = 0$) with an average displacement from that minimum equal to Δ_r .

equivalent length scale, assuming motion parallel to the long axis, is the rod length, L .

In the absence of a time-dependent driving force, $F_{AC} = 0$, the average velocity, v_{AV} , can be extracted deterministically, i.e. ignoring the effects of thermal noise, from (5) and is found to be [63, 64]

$$v_{AV} = \begin{cases} 0, & F_{DC} \leq F_C \\ \frac{1}{\zeta} \sqrt{F_{DC}^2 - F_C^2}, & F_{DC} > F_C. \end{cases} \quad (8)$$

In the presence of a time-dependent driving force [56, 57], there is potential for the particle to exhibit dynamic mode locked motion if $v_{AV} \approx n\lambda\nu$, where n is an integer. If this is satisfied then

$$v_{AV} = n\lambda\nu, \quad (9)$$

which gives a constant average velocity despite small variations in the average driving velocity.

2.4. Subcritical driving

When driven at a constant driving force below the critical driving force a particle is confined to a single optical trap and its average velocity, v_{AV} , is zero. However, the particle does not simply remain in the centre of an optical landscape minimum. The displacement from this minimum, Δ_r , is shown schematically in figure 2 and can be found by considering the force balance with $F_{DC} = -F_{opt}$ which can be written as

$$F_{DC} = F_C \sin\left(\frac{2\pi x}{\lambda}\right). \quad (10)$$

For a driving velocity $v_{DC} = F_{DC}/\zeta$, this equilibrium displacement, $\langle x(v_{DC}) \rangle \equiv \Delta_r(v_{DC})$, is found as

$$\Delta_r = \frac{\lambda}{2\pi} \arcsin\left(\frac{\zeta v_{DC}}{F_C}\right). \quad (11)$$

This distance can be directly calculated if $\zeta \neq \zeta(\Delta_r)$. However, in a regime where $\zeta = \zeta(\Delta_r)$ due to close proximity to a wall, as discussed in section 2.2, then this dependence can be probed by using the following relation,

$$\frac{\zeta}{F_C} = \frac{1}{v_{DC}} \sin\left(\frac{2\pi\Delta_r}{\lambda}\right), \quad (12)$$

which quantifies the drag coefficient as a function of distance from the centre of an optical trap.

3. Experimental methods

3.1. Colloidal model system and experimental setup

The colloidal model system used consists of silica rods dispersed in deionised water in a quartz glass Hellma cell (internal cavity, 20 mm × 9 mm × 200 μm). The particles have a higher density than the surrounding solvent so sediment to the bottom of the cell. The system is sufficiently dilute to ensure that there is only a single particle in the field of view at any time. Rods vary in length and width, but typically rods are chosen to have $L \approx 4 \mu\text{m}$ and $W \approx 0.5 \mu\text{m}$ so that the rods can be imaged and optically manipulated.

Colloidal spheres are used as a reference and these are Dynabeads M-270 carboxylic acid that have a diameter of 3 μm when dispersed in 20% EtOH(aq) in a quartz glass Hellma cell [56]. The particles are manipulated using optical traps formed with a 1064 nm infrared laser, controlled by a pair of perpendicular acousto-optical deflectors, and focused using a 50×, NA = 0.55 objective, as described in [65]. Note that the laser light enters the system from above and scattering forces act in the same direction as gravity.

3.2. Equilibrium trap measurements

A thermal equilibrium method is used to find the stiffness constant of an optical trap by taking a long time series of a Brownian particle held by an optical trap close to a wall [3]. The images obtained are then analysed to give a probability distribution of the displacement of the particle from the trap centre. This is used to obtain a potential energy curve using $P(x) \propto \exp(-U(x)/k_B T)$. To achieve this a colloidal rod is trapped and imaged at 10 fps for 30 min. The optical trap used here is generated using a laser output power of 80 mW, which was chosen to allow stable optical trapping of a rod in both the horizontal and vertical configurations. At higher laser powers, only the vertical configuration is seen while at lower laser powers, a rod cannot be confined within the optical trap. Note that the focus of the optical trap was held at the same height during the experiments, relatively close to the bottom surface of the sample cell.

The images of the rods are analysed to obtain the rod orientation. To this end, the particles are located using an initial binarisation with an ellipsoid fitted to the resulting image. The centre of mass is found at the centre of the ellipsoid and vertical and horizontal rods are separated using the projected rod length. A rod is categorised as horizontal if the projected rod length is greater than 1.5 μm and vertical otherwise. This crude separation works well due to the fact that a rod spends almost all of its time either in a fully horizontal or vertical orientation.

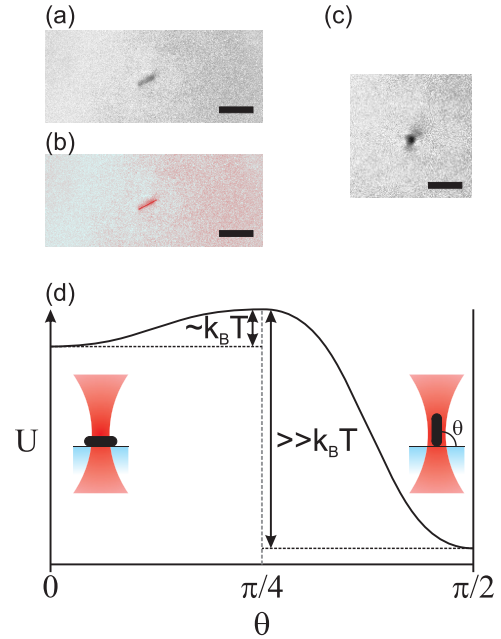


Figure 3. (a) Microscope image of a horizontal rod imaged from below, which is tracked in (b) with the rod's major axis shown in red. (c) Microscope image of a vertical rod. This appears roughly spherical as it is viewed from below with some distortion due to optical effects. Scale bars are 5 μm. (d) Schematic plot of potential energy as a function of the angle between the rod and the wall, θ .

3.3. Average velocity measurements

As a rod is driven through an optical landscape it is imaged at 10 fps. The rod is tracked to give $x(t)$ from which $v(t)$ and $v(x)$ can subsequently be determined. The optical landscape is made up of 12 optical traps with a spacing of $\lambda = 6 \mu\text{m}$ and a total laser intensity of $I_0 = 960 \text{ mW}$. This results in the same laser intensity per trap as is used for the single trap measurements. In experiments where the sample is subject to a driving velocity, a rod is always in a horizontal configuration and if it moves into a vertical configuration the experiment is restarted because in this configuration the particle cannot pass through the landscape due to its greatly enhanced trap stiffness. A rod is driven using a constant driving force and subsequently also with a modulated driving force using a PI-542.2CD piezo-stage, controlled using LabView [56, 57]. The magnitude of the oscillations used is $F_{AC}/\zeta = v_{AC} = 5.2 \mu\text{m s}^{-1}$ with an associated frequency of $\nu = 0.5 \text{ Hz}$.

To enable a direct comparison, a sphere is driven with a constant driving velocity across an optical landscape consisting of 46 optical traps with a spacing of $\lambda = 4 \mu\text{m}$ and $I_0 = 350 \text{ W}$. These experimental parameters lead to comparable critical velocities for both the rod ($v_C = F_C/\zeta = 3.8 \mu\text{m s}^{-1}$) and the sphere ($v_C = 2.8 \mu\text{m s}^{-1}$).

4. Results and discussion

4.1. Equilibrium trapping of colloidal rods in a single optical trap

First, the trapping behaviour of a single rod in a single optical trap, whose focus was held at the same height during the

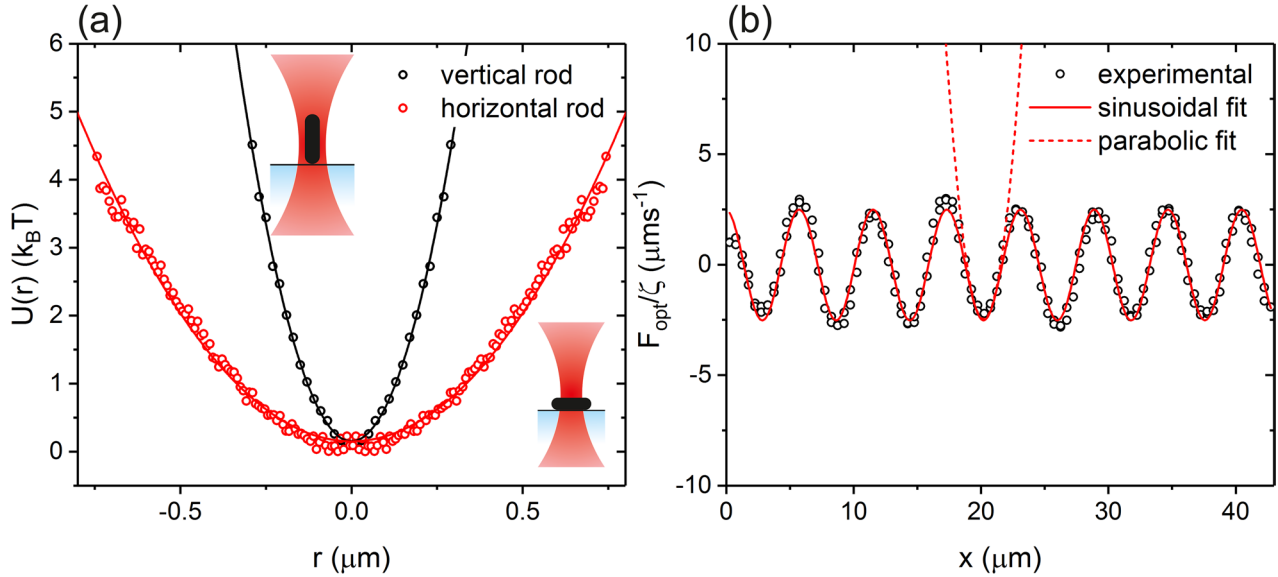


Figure 4. (a) A comparison of the optical potential experienced by a horizontal (red) and vertical (black) rod confined by a single optical trap. Experimental data is shown by points. Solid lines show a parabolic fit to both sets of data, from which the trapping stiffness can be extracted. This data is shown for a single rod, averaged over time. (b) The sinusoidal potential energy surface experienced by a rod driven through a line of optical traps with a spacing of $6 \mu m$. A parabolic fit is also shown for one potential well and close to the minima gives a good description of the true optical landscape.

experiment, is characterised. An optically trapped colloidal rod close to a wall exhibits two ‘metastable’ trapping configurations, horizontal and vertical, which are shown in figures 3(a)–(c). A schematic showing the relative stability of these configurations is shown in figure 3(d) and is such that a horizontal rod may overcome the effects of gravity and the scattering forces to leave it in a vertical configuration where it will remain. It is not possible to experimentally measure $U(\theta)$ using the technique described in section 3.2 due to the irreversibility of the transition from a horizontal to a vertical configuration. The transition from a horizontal to a vertical configuration is more prevalent for smaller rods where the effects of gravity and scattering are reduced so that the activation energy required to switch configurations is reduced.

A comparison between the optical potentials of the vertical and horizontal states is shown in figure 4(a). Both states exhibit a parabolic optical potential energy landscape centered at the focus of the optical trap but clearly exhibit a differing trap stiffness. The fact that a vertical rod exhibits a parabolic optical potential energy landscape is expected, as it has a circular cross section, the same as for a sphere. A horizontal rod, however, has an anisotropic cross section, yet a parabolic potential energy curve is found when the particle is isolated in an optical trap. This is due to the fact that the rod can freely rotate in the xy -plane, meaning that on average it has a circular cross section similarly to a sphere. Assuming a harmonic potential [3, 16], a spring constant is extracted and is found to be seven times higher for the vertical rod than for the horizontal rod ($k_{vertical} = 3.7 \times 10^{-6} \text{ kg s}^{-2}$, $k_{horizontal} = 5.5 \times 10^{-7} \text{ kg s}^{-2}$). This is attributed to the fact that in the vertical state, there is a larger overlap between the particle and laser light, so it experiences a stronger optical force, leading to an increased trap stiffness.

4.2. Driven colloidal rods in optical potential energy landscapes

Next, we consider the behaviour of a colloidal rod in a more complex optical potential energy landscape composed of multiple equally spaced optical traps. First, the optical potential energy landscape is characterised by driving a rod well above the critical velocity and tracking the observed velocity, from which F_{opt}/ζ can be calculated [57]. The resulting optical force is plotted as a function of position in figure 4(b) and is clearly sinusoidal as is seen for a sphere [65]. Potential minima are regularly spaced by a distance of $\lambda = 6 \mu m$, which is the spacing of optical traps as described in section 2.3.

4.2.1. Subcritical driving. A particle driven below the critical velocity, $v_{DC} < v_C$, will remain confined to a single optical trap. In this regime, the average particle velocity is $v_{AV} = 0$ but information can be gained about the drag coefficient of a particle, ζ , by plotting the average displacement from the centre of a trap as a function of the driving velocity as is shown in figure 5(a). Here the results obtained for a sphere are also shown for comparison. The particle displacement, Δ_r , increases with the driving velocity for both a sphere and a rod as the particle can translate further from a landscape minimum before equilibrium is reached at $F_{DC} = -F_{opt}$. A sphere shows an increase in Δ_r as driving velocity is increased, and diverges as v_{DC} tends towards v_C . This behaviour is well described by (11), which is also plotted. Conversely, the value of Δ_r for a rod reaches a plateau as v_{DC} approaches v_C which suggests that the drag coefficient of a rod is not simply a constant, but instead that $\zeta = \zeta(\Delta_r)$. This can be probed by noting that the right hand side of (12) can be evaluated and is directly proportional to the drag coefficient, ζ . As F_C is a feature of the optical landscape and constant, (12) can now be used to plot

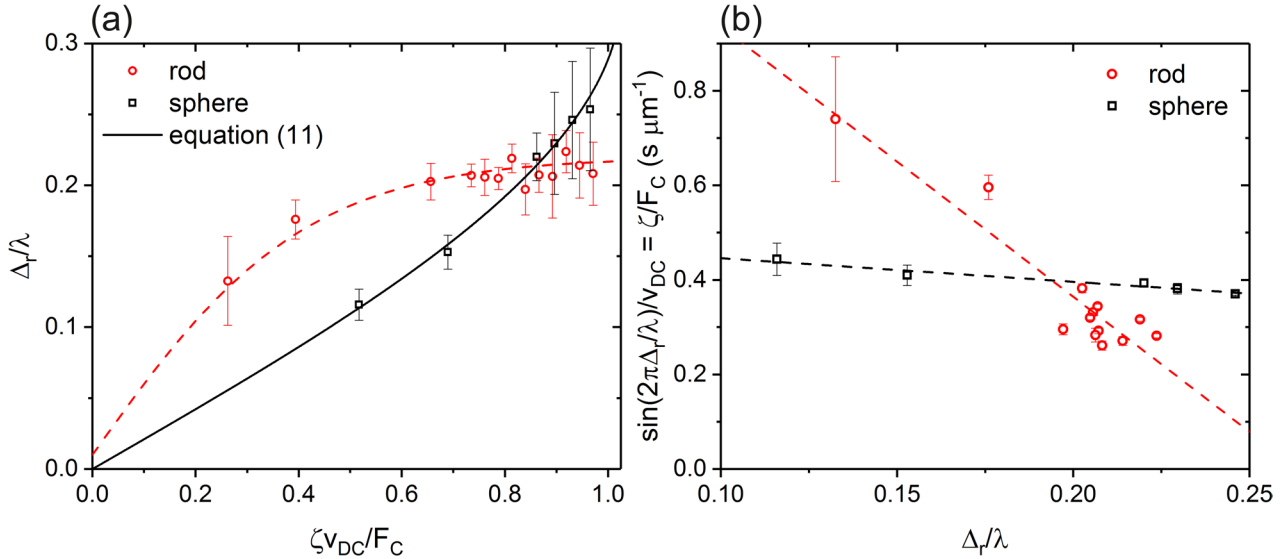


Figure 5. (a) A plot showing the driving velocity dependence of the equilibrium distance of a particle from the centre of an optical trap. For a sphere (black points) a fit to (11) is shown (black line). For a rod (red points) the behaviour deviates from (11) and the dashed red line simply acts as a guide to the eye. (b) A plot of the drag coefficient as calculated from (12) against distance from the centre of an optical trap. The dashed lines are guides to the eye.

the change of the drag coefficient as a function of Δ_r as is shown for a rod and a sphere in figure 5(b). The drag coefficient of the rod is highly dependent on its displacement from the centre of an optical trap, Δ_r . As the rod moves further from a minimum of the optical landscape, the drag coefficient reduces by a significant amount. We also note that the drag coefficient of the sphere is influenced by its proximity to an optical trap but to a far lesser extent than for the rod.

The drag coefficients of a sphere and a rod are influenced by the presence of a wall [61, 66] and this effect is enhanced when a particle is subject to scattering forces from an optical trap. The scattering forces act to push the particle towards the surface and therefore increase the interactions between the particle and the surface. The rods used here have a larger equilibrium distance from the wall than a sphere in the absence of an optical trap due to an increased gravitational height, l_g ($l_{g,sphere} \approx 50 \text{ nm}$, $l_{g,rod} \approx 1 \text{ } \mu\text{m}$). This means that in the presence of an optical trap the reduction in distance between the rod and wall is greater than the equivalent reduction in distance for a sphere. This combined with a higher dependence on proximity to a wall [61, 66] leads to a larger increase of the drag coefficient for a rod in the presence of an optical trap. Here a quantitative analysis of ζ is not possible due to a lack of information about the absolute distance between the particle and the wall.

4.2.2. Supercritical driving. A rod becomes mobile when driven through an optical landscape at velocities above the critical velocity, $v_{DC} > v_C$. By tracking the particle motion, trajectories are obtained such as those shown in figure 6(a) for four different driving velocities. For the lowest driving velocity shown, $v_{DC} = 2.5 \text{ } \mu\text{m s}^{-1}$, the particle is below the critical velocity and is therefore confined to a single minimum in the optical landscape and does not deviate from $x = 0$ other than small fluctuations due to Brownian noise. As the

driving velocity is increased to $v_{DC} = 4.0 \text{ } \mu\text{m s}^{-1}$, the particle is able to escape the initial minimum in the optical landscape and travels a finite distance. As the driving velocity further increases to $v_{DC} = 5.0 \text{ } \mu\text{m s}^{-1}$ and $v_{DC} = 8.0 \text{ } \mu\text{m s}^{-1}$, so does the gradient of the trajectory, indicating a higher average particle velocity. In addition, there is evidence of the optical landscape in the trajectories, as there is a noticeable drop in the velocity of a rod at intervals of $6 \text{ } \mu\text{m}$, corresponding to the wavelength of the optical landscape. At higher driving velocities, the particle spends less time on average being confined to a single minimum in the optical landscape.

From these trajectories the average particle velocity is obtained using $v_{AV} = \Delta x / \Delta t$. In figure 6(b) the average velocity is plotted as a function of the driving velocity. Particles remain stationary below the critical velocity, after which they show an increase in the average velocity as the driving velocity increases. At high driving velocities the behaviour tends towards that seen in the absence of any optical landscape because $F_{DC} \gg F_{opt}$. The average velocity is fitted using (8) which shows good agreement with the measured average velocity. Deviations from this deterministic equation for v_{AV} are seen close to the critical velocity due to Brownian noise. This provides the particle with enough thermal energy to overcome the barrier to motion slightly below the critical velocity for the deterministic case [63, 64, 67].

4.2.3. Modulated driving force. Next, the motion of a rod driven by a more complex, time-dependent driving velocity over an optical landscape is described. Experimental trajectories of a rod are shown in figure 7(a) for three different average driving velocities. Each trajectory shows a clear signature of the oscillations in the driving velocity at $n \times t\nu$, where n is an integer. This is marked by the vertical dashed lines in figure 7(a). For the lowest driving velocity shown here, $v_{DC} = 4.8 \text{ } \mu\text{m s}^{-1}$, the particle exhibits some forward

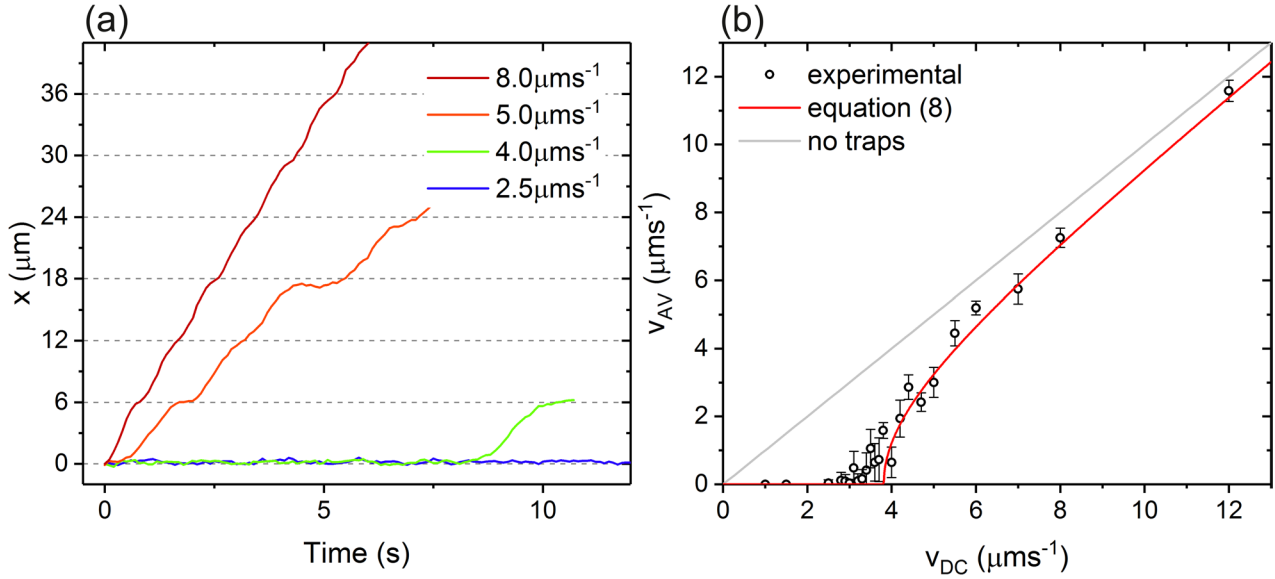


Figure 6. (a) Trajectories of a rod driven through an optical landscape, $\lambda = 6 \mu\text{m}$, at different driving velocities. (b) The average particle velocity plotted against the driving velocity. Experimental data (black circles) is fitted with (8) [62] (red line). For reference, the behaviour expected in the absence of an optical landscape is shown (grey line) and shows $v_{AV} = v_{DC}$.

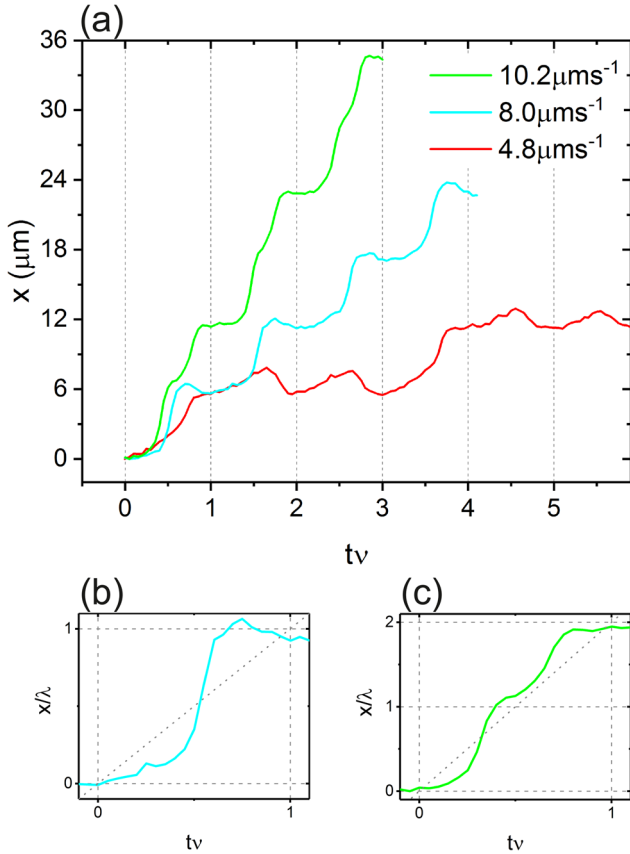


Figure 7. (a) An example of trajectories of a rod subject to an oscillating driving force where $\lambda = 6 \mu\text{m}$, $v_{AC} = 5.2 \mu\text{m s}^{-1}$ and $\nu = 0.5 \text{ Hz}$ for three different average driving velocities. Zoomed in trajectories are shown for (b) $8.0 \mu\text{m s}^{-1}$ and (c) $10.2 \mu\text{m s}^{-1}$ to highlight periodic motion of these trajectories.

motion and moves the distance of $\Delta x = 2\lambda = 12 \mu\text{m}$ in the observed period. The imposed oscillations cause the particle to rock back and forth within a single minima before the

particle escapes and passes to the next optical trap. As the driving velocity is increased to $v_{DC} = 8.0 \mu\text{m s}^{-1}$, a much more coherent motion is observed and within each period, the particle moves a distance of $\Delta x = \lambda$. This is highlighted in figure 7(b) for a single period and is termed the (1,0) mode to denote the fact that a particle moves forward one wavelength and has no backward motion per period [56]. At the highest driving velocity of $v_{DC} = 10.2 \mu\text{m s}^{-1}$, the particle is being driven at a high enough driving velocity to move $\Delta x = 2\lambda$ for each oscillation of the driving velocity. This causes the particle velocity to show a sharp rise as the particle begins to move out of the trap to which it is originally confined. It then slows as it passes into the first trap before the particle velocity increases again corresponding to the particle moving into the second trap. This motion is shown more clearly in figure 7(c) and corresponds to the (2,0) mode [56].

A plot of the average particle velocity as a function of the average driving velocity is shown in figure 8(a). At a low average driving velocity, the average particle velocity is zero before an increase in average velocity above $v_{DC} \approx 4 \mu\text{m s}^{-1}$ is seen. The average particle velocity increases until $v_{DC} \approx 6.8 \mu\text{m s}^{-1}$, at which point the average particle velocity reaches a plateau until $v_{DC} \approx 8.8 \mu\text{m s}^{-1}$. Above this, the average particle velocity then steadily increases for measured values up to $v_{DC} = 10.2 \mu\text{m s}^{-1}$.

The trajectory for $v_{DC} = 8.0 \mu\text{m s}^{-1}$ in figure 7(a) already suggests the presence of dynamic mode locking and in this regime, the rod is expected to have an average velocity $v_{AV} = n\lambda\nu$, where n is an integer. This is initially seen at low driving velocities where $n = 0$, corresponding to $v_{AV} = 0$, and is termed the zeroth mode locked step. The first mode locked step is reached at $v_{DC} \approx 6.8 \mu\text{m s}^{-1}$, corresponding to $v_{AV} = \lambda\nu = 3 \mu\text{m s}^{-1}$. This physically corresponds to the particle travelling a distance equal to the wavelength (see figure 7(b)) of the optical landscape at a frequency identical

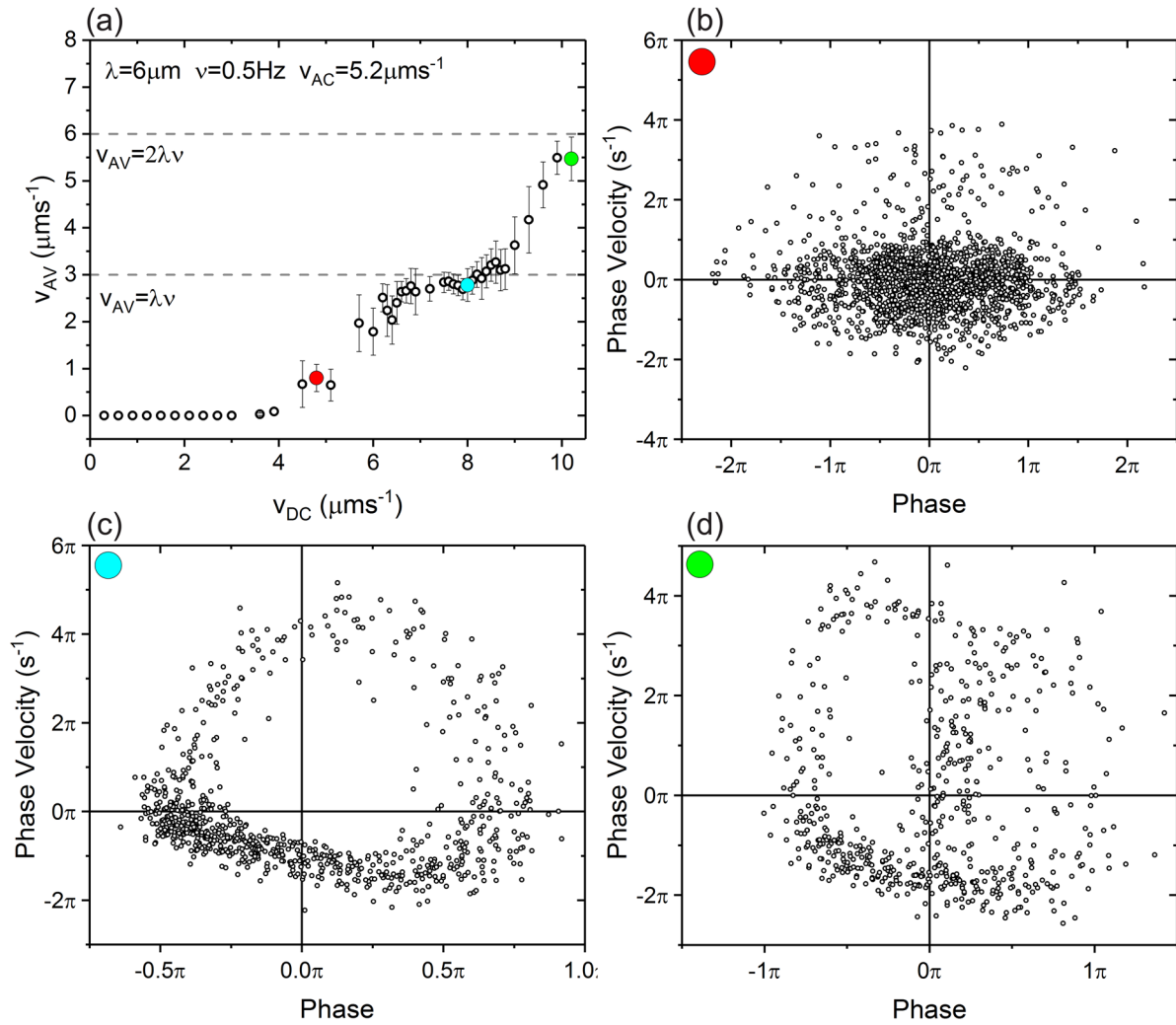


Figure 8. (a) The average particle velocity as a function of the average driving velocity in the presence of a modulated driving force. Experimental parameters are $\lambda = 6 \mu\text{m}$, $\nu = 0.5 \text{ Hz}$, $v_{AC} = 5.2 \mu\text{m s}^{-1}$. The dashed lines show the predicted average velocity of the mode locked steps. The phase portraits for (b) $4.8 \mu\text{m s}^{-1}$, (c) $8.0 \mu\text{m s}^{-1}$, and (d) $10.2 \mu\text{m s}^{-1}$ are shown with the corresponding points in (a) highlighted by the filled data points.

to the externally imposed frequency, 0.5 Hz . As the driving velocity is further increased, it leaves the mode locked regime at $v_{DC} \approx 8.8 \mu\text{m s}^{-1}$ and again increases in average velocity where it approaches the average velocity predicted for the second mode locked step. We note that the mode locking behaviour of the rods is very similar to that exhibited by spheres [56, 57], which suggests that the spatial dependence of the rod's drag coefficient (figure 5) does not significantly affect its dynamics.

Another way to represent the periodic, mode locked motion is with the use of phase portraits [56]. In figures 8(b)–(d) the phase portraits associated with the coloured points in figure 8(a) are plotted, which also correspond to the trajectories shown in figure 7(a). Figure 8(b) shows the phase portrait for $v_{AV} = 4.8 \mu\text{m s}^{-1}$ where a particle is not dynamically mode locked. Here the phase portrait does not correspond to a closed loop as the particle does not exhibit synchronised motion. In contrast, figure 8(c) shows the phase portrait for $v_{AV} = 8.0 \mu\text{m s}^{-1}$, which lies on the first mode locked step and clearly shows a closed loop, the signature of dynamic mode

locking [56]. The closed nature denotes the periodic motion that corresponds to a particle translating to the neighbouring minimum each time the stage oscillates. This plot is formed from multiple trajectories, capturing a particle crossing 40 minima in the potential energy landscape while the stage oscillates. Each oscillation leads to a closed loop that, when overlaid, accentuates the predictable motion of the particle at this velocity. Figure 8(d) is the phase portrait for $v_{AV} = 10.2 \mu\text{m s}^{-1}$, which falls close to where the second mode locked step is expected. As this is not truly on a mode locked step, the noise greatly affects the phase portrait but the almost closed loop nature of the phase portrait gives evidence that this is the onset of the second mode locked step.

5. Conclusions

Here the static and dynamic behaviour of colloidal rods in an optical potential energy landscape has been studied. Initially the stable states of a single colloidal rod in a single optical trap close to a wall were explored. Two metastable states,

corresponding to a horizontal or vertical rod were observed. A vertical rod was trapped more effectively than a horizontal rod with both experiencing a parabolic potential energy landscape. Next, the motion of a driven colloidal rod in a one-dimensional optical potential energy landscape was studied. The equilibrium position of a particle was investigated as it was driven below the critical velocity and confined to a single potential energy minimum of the optical landscape. The equilibrium position of a rod was found to vary substantially from that of a sphere due to the drag coefficient of a rod being dependent on its proximity to an optical trap. The driving velocity was then increased above the critical velocity to allow the particle to traverse the optical landscape. Here, the average particle velocity increased as the square root of the driving velocity. Finally, oscillations were introduced to the driving velocity and rod trajectories were analysed. The rods exhibited dynamic mode locking behaviour similar to that observed for spheres [56, 57], and the synchronised motion was characterised with the use of phase portraits.

Acknowledgments

Louis Cortes and Arran Curran are thanked for useful discussions. The EPSRC is acknowledged for financial support. YG acknowledges financial support from FP7-PEOPLE (PIIF-GA-2012-327919) and from the National Natural Science Foundation of China (Project No. 11774237).

ORCID iDs

Roel P A Dullens  <https://orcid.org/0000-0003-1751-0958>

References

- [1] Ashkin A, Dziedzic J M, Bjorkholm J E and Chu S 1986 *Opt. Lett.* **11** 288–90
- [2] Ashkin A 1970 *Phys. Rev. Lett.* **24** 24–7
- [3] Neuman K C and Block S M 2004 *Rev. Sci. Instrum.* **75** 2787–809
- [4] Rohrbach A 2005 *Phys. Rev. Lett.* **95** 168102
- [5] Jahnelt M, Behrndt M, Jannasch A, Schäffer E and Grill S W 2011 *Opt. Lett.* **36** 1260–2
- [6] Jones P H, Maragó O M and Volpe G 2015 *Optical Tweezers Principles and Applications* (Cambridge: Cambridge University Press)
- [7] MacDonald M P, Spalding G C and Dholakia K 2003 *Nature* **426** 421–4
- [8] Ladavac K, Kasza K and Grier D G 2004 *Phys. Rev. E* **70** 010901
- [9] Pelton M, Ladavac K and Grier D G 2004 *Phys. Rev. E* **70** 031108
- [10] Xiao K and Grier D G 2010 *Phys. Rev. E* **82** 051407
- [11] Tassieri M et al 2015 *Sci. Rep.* **5** 8831
- [12] Furst E M and Squires T M 2017 *Microrheology* (Oxford: Oxford University Press)
- [13] Kellermayer M S, Smith S B, Granzier H L and Bustamante C 1997 *Science* **276** 1112–6
- [14] Dholakia K, Spalding G and MacDonald M 2002 *Phys. World* **15** 31–5
- [15] Grier D G 2003 *Nature* **424** 810–6
- [16] Dholakia K, Reece P and Gu M 2008 *Chem. Soc. Rev.* **37** 42–55
- [17] Wördemann M 2012 *Structured Light Fields: Applications in Optical Trapping, Manipulation, and Organisation* (Berlin: Springer)
- [18] Higurashi E, Ukita H and Tanaka H 1994 *Appl. Phys. Lett.* **64** 2209–10
- [19] Lapointe C P, Mason T G and Smalyukh I I 2011 *Opt. Express* **19** 18182–9
- [20] Glotzer S C and Solomon M J 2007 *Nat. Mater.* **6** 557–62
- [21] Hernandez C J and Mason T G 2007 *J. Phys. Chem. C* **111** 4477–80
- [22] Simpson S H 2014 *J. Quantum Spectrosc. Radiat. Trans.* **146** 81–99
- [23] Sacanna S, Korpics M, Rodriguez K, Colón-Meléndez L, Kim S H, Pine D J and Yi G R 2013 *Nat. Commun.* **4** 1688
- [24] Frenkel D, Lekkerkerker H N W and Stroobants A 1988 *Nature* **332** 822–3
- [25] Bolhuis P and Frenkel D 1997 *J. Chem. Phys.* **106** 666–87
- [26] Dogic Z and Fraden S 2006 *Curr. Opin. Colloid Interface Sci.* **11** 47–55
- [27] Savenko S V and Dijkstra M 2004 *Phys. Rev. E* **70** 051401
- [28] Grelet E 2008 *Phys. Rev. Lett.* **100** 168301
- [29] Gasser U 2009 *J. Phys.: Condens. Matter* **21** 203101
- [30] Kuijk A, Van Blaaderen A and Imhof A 2011 *J. Am. Chem. Soc.* **133** 2346–9
- [31] Kuijk A, Byelov D V, Petukhov A V, Van Blaaderen A and Imhof A 2012 *Faraday Discuss.* **159** 181–99
- [32] Lekkerkerker H N W and Vroege G J 2013 *Phil. Trans. R. Soc. A* **371** 20120263
- [33] Kuijk A, Troppenz T, Filion L, Imhof A, van Roij R, Dijkstra M and Van Blaaderen A 2014 *Soft Matter* **10** 6249–55
- [34] Cortes L B G, Gao Y, Dullens R P A and Aarts D G A L 2017 *J. Phys.: Condens. Matter* **29** 064003
- [35] De Braaf B, Oshima Menegon M, Paquay S and Van der Schoot P 2017 *J. Chem. Phys.* **147** 244901
- [36] Van der Kooij F M and Lekkerkerker H N 2000 *Phys. Rev. Lett.* **84** 781–4
- [37] Löwen H 2008 *J. Phys.: Condens. Matter* **20** 404201
- [38] Kang K and Dhont J K G 2010 *Soft Matter* **6** 273–86
- [39] Gao Y, Romano F, Dullens R P A, Doye J K and Aarts D G A L 2018 *Phys. Rev. Mater.* **2** 015601
- [40] Van der Zande B M I, Koper G J and Lekkerkerker H N W 1999 *J. Phys. Chem. B* **103** 5754–60
- [41] Lewis A H, Garlea I, Alvarado J, Dammone O J, Howell P D, Majumdar A, Mulder B M, Lettinga M P, Koenderink G H and Aarts D G A L 2014 *Soft Matter* **10** 7865–73
- [42] Gray G W and Kelly S M 1999 *J. Mater. Chem.* **9** 2037–50
- [43] Ashkin A and Dziedzic J 1987 *Science* **235** 1517–20
- [44] Agarwal R, Ladavac K, Roichman Y, Yu G, Lieber C M and Grier D G 2005 *Opt. Express* **13** 8906–12
- [45] Di Leonardo R, Cammarota E, Bolognesi G, Schäfer H and Steinhart M 2011 *Phys. Rev. Lett.* **107** 044501
- [46] Mihiretie B M, Snabre P, Loudet J C and Pouligny B 2014 *Eur. Phys. J. E* **37** 124
- [47] Kuhn S, Kosloff A, Stickler B A, Patolsky F, Hornberger K, Arndt M and Millen J 2017 *Optica* **4** 356–60
- [48] Simpson S H and Hanna S 2011 *J. Opt. Soc. Am. A* **28** 850–8
- [49] Simpson S H and Hanna S 2010 *J. Opt. Soc. Am. A* **27** 1255–64
- [50] Cheong F C and Grier D G 2010 *Opt. Express* **18** 6555–62
- [51] Sancho J M and Lacasta A M 2010 *Eur. Phys. J. Spec. Top.* **187** 49–62
- [52] Korda P T, Taylor M B and Grier D G 2002 *Phys. Rev. Lett.* **89** 128301
- [53] Bohlein T and Bechinger C 2012 *Phys. Rev. Lett.* **109** 058301
- [54] Bohlein T, Mikhael J and Bechinger C 2012 *Nat. Mater.* **11** 126–30

- [55] Brazda T, Silva A, Manini N, Vanossi A, Guerra R, Tosatti E and Bechinger C 2018 *Phys. Rev. X* **8** 011050
- [56] Juniper M P N, Straube A V, Besseling R, Aarts D G A L and Dullens R P A 2015 *Nat. Commun.* **6** 7187
- [57] Juniper M P N, Zimmermann U, Straube A V, Besseling R, Aarts D G A L, Löwen H and Dullens R P A 2017 *New J. Phys.* **19** 013010
- [58] Brazda T, July C and Bechinger C 2017 *Soft Matter* **13** 4024–8
- [59] Buzzaccaro S, Tripodi A, Rusconi R, Vigolo D and Piazza R 2008 *J. Phys.: Condens. Matter* **20** 494219
- [60] Yang K, Lu C, Zhao X and Kawamura R 2017 *PLoS One* **12** e0188015
- [61] Padding J T and Briels W J 2010 *J. Chem. Phys.* **132** 054511
- [62] Juniper M P N, Straube A V, Aarts D G A L and Dullens R P A 2016 *Phys. Rev. E* **93** 012608
- [63] Reimann P, Van den Broeck C, Linke H, Hänggi P, Rubi J M and Pérez-Madrid A 2001 *Phys. Rev. Lett.* **87** 010602
- [64] Reimann P, Van den Broeck C, Linke H, Hänggi P, Rubi J M and Pérez-Madrid A 2002 *Phys. Rev. E* **65** 031104
- [65] Juniper M P N, Besseling R, Aarts D G A L and Dullens R P A 2012 *Opt. Express* **20** 28707
- [66] Svoboda K and Block S M 1994 *Annu. Rev. Biophys. Biomol. Struct.* **23** 247–85
- [67] Gitterman M 2008 *The Noisy Pendulum* (Singapore: World Scientific)